*energies*

MDPI

*Article*

# Energy Efficiency Analysis of Pumping Systems Impacted by the Golden Mussel: A Case Study in the Brazilian Amazon

**Tâmara Rita Costa de Souza [1,*], Jennifer Thayane Melo de Andrade [2], Rodrigo Otávio Peréa Serrano [3], Teofânia Heloísa Dutra Amorim Vidigal [1,4], Edna Maria de Faria Viana [1,5], Adriano Silva Bastos [6] and Carlos Barreira Martinez [1,6]**

1 Graduate Program in Mechanical Engineering, Department of Mechanical Engineering, Federal University of Minas Gerais, Belo Horizonte 31270-901, Brazil
2 Postgraduate Program in Zoology, Department of Zoology, Institute of Biological Sciences, Federal University of Minas Gerais, Belo Horizonte 31270-901, Brazil
3 Postgraduate Program in Science, Innovation and Technology for the Amazon and Postgraduate Program in Geography, Federal University of Acre, Rio Branco 69920-900, Brazil
4 CPH (Centro de Pesquisas Hidráulicas), Laboratory of Malacology, Department of Zoology, Institute of Biological Science and LELF (Laboratory studys of the *Limnoperna fortunei*), Federal University of Minas Gerais, Belo Horizonte 31270-901, Brazil
5 Department of Hydraulic Engineering and Water Resources, Federal University of Minas Gerais, Belo Horizonte 31270-901, Brazil
6 Thermo-Hydroelectro Laboratory, Institute of Mechanical Engineering, Federal University of Itajubá, Itajubá 35903-087, Brazil
* Correspondence: tamararccosta@hotmail.com; Tel.: +55-31-9-9553-8667

**Abstract:** Pumping systems, especially those used in the water supply sector and in industrial and hydroelectric facilities, are commonly infested by the golden mussel. This causes an increase in maintenance operations (e.g., system shutdowns for cleaning) that can generate an increased energy cost. The geographical expansion of the golden mussel in Latin America presents an economic risk, not only to the ecosystem in general, but also to the energy sector. The imminence of its spread in the Amazon region, one of the main river basins in South America, is cause for concern with regard to the problems that bioinvasion of this species can cause. Given the absence of studies on the loss of energy efficiency in pumping systems impacted by the golden mussel, this study proposes a methodology to estimate the increase in energy consumption and costs of pumping under such bioinfestation. For the standardization of the methodology and development of mathematical calculations (both novel and improved equations), data from the literature (the growth of the golden mussel as a function of infestation time) and an analysis of the dimensions (length and height) of a sample of mussels available in the laboratory were considered. These data were used to calculate the roughness generated by the mussel infestation in the pumping suction and discharger pipe, which was necessary to determine the loss of energy efficiency (load loss, power consumption, and cost of pumping) resulting from the increase in energy consumption for pumping. This methodology was applied to a pumping station representative of the Brazilian Amazon as a case study. The results show an average increase in economic indicators (consumption and cost of pumping) after the system undergoes bioinfestation. This total increase corresponded to 19% and 44% in the first and second years, respectively, achieving a stabilization of the increase in the cost of pumping at 46%, in the 30 months of operation. Our results demonstrate the pioneering nature of the proposal, since these are the first quantitative data on the energy efficiency of pumping systems associated with bioinfestation by the golden mussel. These results can also be used to estimate the increase in costs caused by golden mussel bioinfestation in the raw water pumping systems of other facilities.

**Keywords:** biofouling; bioinfestation; bioinvasion; energy consumption of pumping; cost of pumping; energy efficiency; golden mussel; load loss; pumping systems



**Citation:** Souza, T.R.C.d.; Andrade, J.T.M.d.; Serrano, R.O.P.; Vidigal, T.H.D.A.; Viana, E.M.d.F.; Bastos, A.S.; Martinez, C.B. Energy Efficiency Analysis of Pumping Systems Impacted by the Golden Mussel: A Case Study in the Brazilian Amazon. *Energies* **2023**, *16*, 1858. https://doi.org/10.3390/en16041858

Academic Editors: Marian Banaś, Krzysztof Kołodziejczyk and Tadeusz Pająk

Received: 18 January 2023
Revised: 5 February 2023
Accepted: 10 February 2023
Published: 13 February 2023

## 1. Introduction

*Limnoperna fortunei* (Dunker, 1857) (Mytilidae), the golden mussel (GM), has gained considerable prominence as a biofouler (fouling organism of underwater surfaces), causing severe damage to ecosystems and human-made industrial facilities (e.g., hydroelectric plants and those in the water supply sector) [1,2]. This invasive alien species (IAS) reaches the phase of attachment to the substrate, pediveliger, between 15 and 21 days [3,4]. It also easily disperses in the environment, through the larval stage, and attaches itself to various types of substrates such as plants, wood, tires, or metal structures [3]. The GM reaches its reproductive potential with a shell length of 6 mm [5], which explains their rapid growth in layers and their densities of up to 15 ind/cm$^2$ [6].

Present in Brazil since 1998 [7], the geographical distribution of the GM is currently concentrated in the south and southeast regions of Brazil, with prospects of expanding its bioinvasion to the Amazon region [8,9]. The Amazon basin consists of one of the largest centers of hydric potential in Brazil [10]. The dispersion of the GM can occur through planktonic larvae, mainly transported by boats or by juvenile and adult specimens attached to various types of substrates [11], which makes the Amazon basin a region with a high risk of bioinvasion, considering that this basin is widely navigable and the flow of boats is high [12].

Through bioinfestation, the golden mussel has negatively impacted the operation of fluid–mechanical systems, particularly in the water supply sector and hydroelectric power plants, which may cause increased maintenance costs [1,13]. Some of the main problems caused by GM bioinfestation in industrial systems include: (1) clogged pipelines, which compromises the transport of water, including that in the supply and energy sectors [1,14]; (2) increased load loss caused by the reduction in the free flow diameter in pumping systems [15]; (3) the corrosion and decreased strength of various materials where mussels encrust, caused by the formation of a biofilm [16]; and (4) abrasion caused by the friction of the shells inside pipelines with high water flow [17].

Considering the recognized categorization of ecosystem services (services related to the "benefits that people can obtain from the ecosystem"), from the above, the GM comprises two categories of these services: provisioning services (e.g., the provision of energy or water) and regulating and maintenance services (e.g., water purification) affecting both human well-being and the economy [18].

Recently, the economic costs related to biological invasions in Brazil were, for the first time, estimated by Adelino et al. (2021) [19], using the InvaCost (database) [20] and data from different IAS species, including the GM. Of the 460 invasive alien species present in Brazil, only 16 (aquatic and terrestrial ecosystems) are registered in the InvaCost system, with the GM being the only freshwater species with data that allow an estimation of the economic costs [18]. It was observed that the types of costs associated with the GM are concentrated in the activities of control, prevention, social activities (e.g., hydropower generation), and damage repair. The scarcity of economic indicators available for both the GM and other IAS was considered a factor that hindered the more assertive estimation of economic costs. Estimating these costs can help detect areas that may be more economically impacted and help define priority actions [19].

To fill the existing gaps on the impact of the GM on ecosystem services and their monetization, the aim of this study was to estimate the increase in energy consumption with the consequent loss of energy efficiency of a pumping system, based on a case study of a raw water lifting station.

For a general understanding of this work, it is important to mention that:

(1) The assessment of the loss of energy efficiency due to increased energy consumption is an extensive topic and has been applied to fluid–mechanical systems in general [21]. According to Patterson (1996) [22], one way to evaluate the energy efficiency of a system is to use economic indicators that may be more interesting when it is difficult to obtain reliable technical indicators. Thus, we adopt economic indicators (consumption and cost of pumping) as a way of evaluating the energy efficiency of the infested system, since

consumption and cost are inversely proportional to energy efficiency. (2) Pumping systems are at the center of most human activities [23,24] and represent approximately 20% of world energy consumption [25]. (3) Pumping systems can be built with pipes of different materials, the most common being polyvinyl chloride (PVC), high-density polyethylene (HDPE), cast iron (CI), concrete and steel [26]. (4) These materials may be subject to fouling caused by precipitated sediments from water [27,28], which can cause a loss of energy efficiency due to the increased resistance that fluid encounters [29]. (5) Biofouling also can gradually increase, causing an increase in the roughness of the surface of the internal walls of the pipe, as reported for Dreissena polymorpha (the zebra mussel) [30]. Several issues such as a decrease in the free flow diameter and an elevation of the load loss coefficient, which consequently cause the occlusion of the pipe, were reported by Moody (1944) [31]. These problems are aggravated with the aging of the pipe, as a result of time and exposure to different environmental conditions [32,33].

Despite the importance of assessing the loss of energy efficiency of pumping systems, its relationship with the GM (which encrusts in the pumping system) has not yet been studied. In this case study, an installation in the Acre River was selected, which belongs to the Amazon basin and presents a geomorphology related to the sliding of river banks due to variations in their quota throughout the hydrological year [34]. The raw water pumping system uses pumps positioned on rafts anchored to the riverbanks [35]. In the case of the Acre River, the variation in its quota shows an average amplitude of 8.4 m, which can exceed 14 m as a result of flooding [36].

To evaluate the losses in energy efficiency of the pumping systems affected by the GM, we considered two scenarios: the biofouling-free pumping system and the pumping system under the hypothesis of biofouling in the pipes. The aims of this study were as follows: (1) to elaborate a growth curve of the GM to support pumping system obstruction calculations; (2) to analyze the growth of the specimens, and by correlating the angle of attachment with the time of biofouling (new equations), to estimate the roughness that the pumping system achieves by analyzing the growth of biofouling and determining the thickness of the biofouling (bt); (3) to calculate the load loss factor ($f$) and load loss ($\Delta H$) and the progression of the process to reduce the free flow diameter (improved equations); and 4) to determine the energy consumption and costs of the pumping of a representative elevated pumping station (EPS).

## 2. Materials and Methods

### *2.1. Overview*

This study includes an assessment of the loss of energy efficiency in a pumping system of a known pumping station under the golden mussel (GM) biofouling hypothesis. Some biological information from the GM, constructive data from the target station, and some mathematical engineering parameters were used, all of which influence the performance of the pumping system (e.g., load loss). This set of information was necessary for the construction of new equations, as well as for the improvement of existing equations and to obtain results on the economic indicators that validate the loss of energy efficiency. An overview of the methodology is presented in Figure 1, and details of the procedures are reported throughout this section.

### *2.2. Local Characterization*

To calculate the impacts of biofouling on raw water pumping systems, the Elevated Pumping Station (EPS) II Rio Branco, Acre, Brazil [36], was used as an example. The extant coordinates of the site are 10° 0′35.95″ S/ 67°50′38.08″ W. A view of the pumping system of the pumping station is shown in Figure 2. This pumping system is composed of 3 vertical Francis-type centrifugal pumps and a radial rotor that operates 12 h per day, with an average flow rate of 1100 L/s. It has the capacity of vertical mobility by means of floating surfaces, to be able to adjust to the variations in the water levels of the river. The station

characteristics considered were flow rate (Q), efficiency (η), power (P), free flow diameter (D), length suction and discharge pipe (L), velocity (V), and height (H) (Tables 1 and 2).

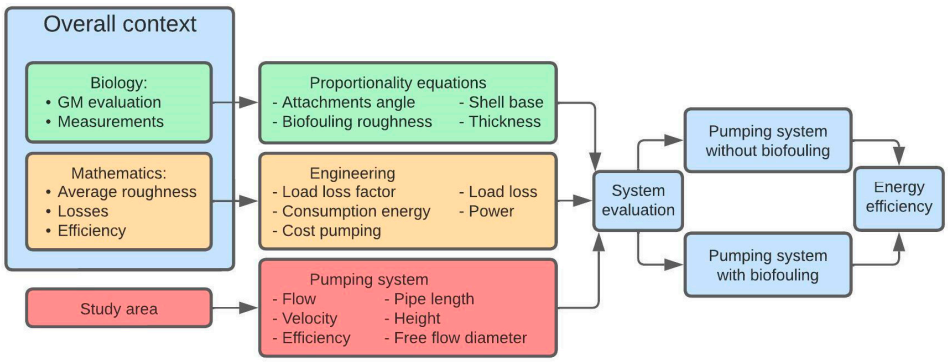


**Figure 1.** Schematic representation of the activities developed in this work.


**Figure 2.** Elevated Pumping Station II, Rio Branco, Acre, consisting of a set of vertical turbine-type pumps. Note: 1—Pump 1; 2—Pump 2; and 3—Pump 3.

**Table 1.** Characteristics of the pipes coupled to the 3 representative pumps adopted to pump from the river to the desander of the river channel—Rio Branco/Acre [36].

| | **Pump 1** | **Pump 2** | **Pump 3** |
|---|---|---|---|
| Q (L/s) | 600 | 300 | 200 |
| η (%) | 78.3 | 70.7 | 77.4 |
| P (CV) | 250 | 150 | 125 |
| D (mm) | 500 | 400 | 300 |
| L (mm) | 71.5 | 73.0 | 72.0 |
| V (m/s) | 3.06 | 2.39 | 2.83 |

The meanings of the symbols are as follows: Q, flow; η, efficiency; P, installed power; L, length of the suction pipe + discharge pipe; D free flow diameter and V, velocity.

**Table 2.** Characteristics of the pumps at the Elevated Pumping Station II, Rio Branco, Acre [36].

| | **Q (L/s)** | **H (mca)** | **η (%)** | | **Q (L/s)** | **H (mca)** | **η (%)** | | **Q (L/s)** | **H (mca)** | **η (%)** |
|---|---|---|---|---|---|---|---|---|---|---|---|
| | 100 | 35.0 | 58 | | 50 | 35.0 | 48 | | 50 | 35.0 | 48 |
| | 200 | 33.0 | 64 | | 100 | 33.0 | 63 | | 100 | 33.0 | 63 |
| | 300 | 30.0 | 69 | | 150 | 30.0 | 69 | | 150 | 30.0 | 69 |
| **Pump 1** | 400 | 25.0 | 74 | **Pump 2** | 200 | 25.0 | 74 | **Pump 3** | 200 | 25.0 | 74 |
| | 500 | 20.5 | 76 | | 250 | 20.5 | 75 | | 250 | 20.5 | 75 |
| | 600 | 14.5 | 79 | | 300 | 14.5 | 75 | | 300 | 14.5 | 75 |
| | 700 | 9.0 | 74 | | 350 | 9.0 | 70 | | 350 | 9.0 | 70 |

The meanings of the symbols are as follows: Q, flow; H, height; and η, efficiency.

The *EPS* that was studied follows the simplified model of a water pumping system (Figure 3). In this study, calculations were performed considering the weighted average of the river's elevation quotes. This resulted in a weighted average of 122.85 m and an average gradient of 13.25 m.

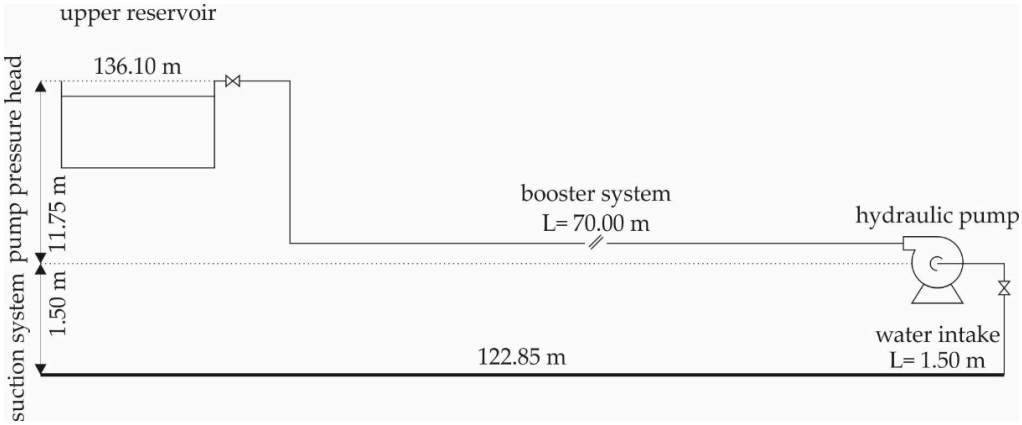


**Figure 3.** Simplified model of the pumping system of the Elevated Pumping Station II, Rio Branco, Acre.

### *2.3. Growth Curve of the Golden Mussel*

The growth curve as a function of time and the GM was obtained through data from the literature (Table 3). It was taken into account that the geometric shape and the location of the attachment in the environment did not have a significant effect on the shell growth of the mussel [37].

**Table 3.** Age and shell length of golden mussel.

| Phase | Length (mm) | Reference | Age (Days) |
|---|---|---|---|
| Egg | 0.080 | [4,38] | 5 |
| Ciliated larvae | 0.080 | | |
| Trochophore Phase 1 | 0.090 | | |
| Trochophore Phase 2 | 0.110 | | |
| Trochophore Phase 3 | 0.125 | | |
| Trochophore Phase 4 | 0.125 | | |
| Larvae D | 0.145 | | |
| Straight hinge Veliger | 0.163 | | |
| Unboned veliger | 0.207 | [4,38] | 16 |
| Pediveliger | 0.239 | | |
| Post larvae | 0.320 | | |
| Post larvae | 20 | [38] | 365 |
| | 30 | [38] | 730 |
| | 35 | [39] | 1095 |
| | 36 | [40] | 1277 |

Source: Adapted from Cataldo et al. [3], Choi and Chim [4], Nakano et al. [38], Boltovskoy and Cataldo [39], and Darrigran and Maroñas [40].

### *2.4. Determination of the Angle of Attachment and the Proportional Relation between Golden Mussel Individuals*

Golden mussels (GMs) were collected in the Itaipu hydroelectric power plant (HPP), which is located in Brazil and Paraguay, 25°24′28″ S, 54°35′24″ W. The GM decomposes rapidly after being removed from the water; accordingly, it was decided to work with dried and sterilized shells. The measured parameters and the angle of attachment were as described by Mackie and Claudi (2010) [41] and Froés et al. (2012) [42], with modifications.

The sample of dried shells containing 1000 specimens of GM went through quartering separation, according to the recommendations of the Brazilian Technical Standard ABNT NBR 10007 [43]. This sample was subdivided into 7 classes, separated according to the shell length of the bivalve, as follows: 0–5 mm, 5–10 mm, 10–15 mm, 15–20 mm, 20–25 mm, 25–30 mm, and >30 mm. Three subsamples, containing 5 individuals in each class, were separated to take the measurements, as shown in Figure 4. After measuring the individuals, the angle of attachment was determined (Figure 4). Then, the rest of the dry shells were artificially attached to surfaces with glue (ASTM-A36 steel), with different materials used in different parts of the HPPs, as reported and used by Simeão (2011) [44]. These artificial attachments were based on the angles of attachment, reproducing the GM attachments that occur in the field. The ASTM-A36 steel surfaces to which shells were artificially attached were photographed for further analysis (see below).

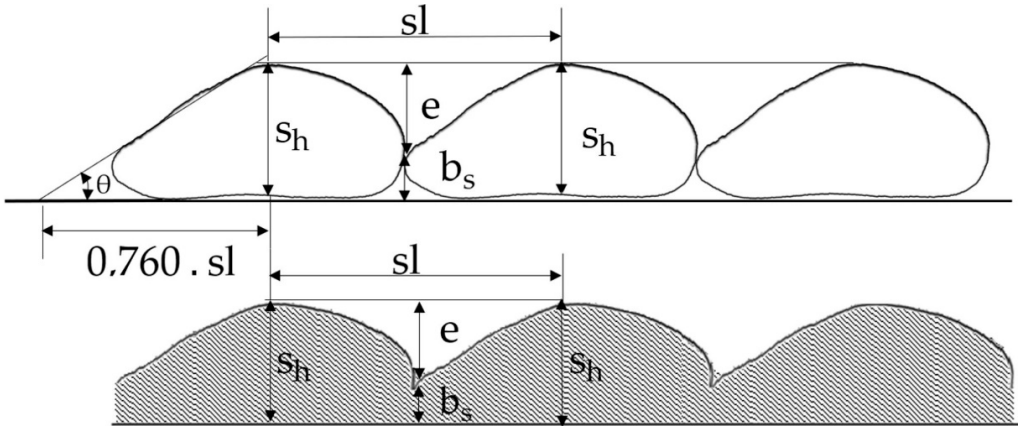


**Figure 4.** Description of how the golden mussel was measured, dimensions provided in mm.

The three previously separated subsamples were examined and their dimensions were surveyed and composed a database containing the dimensions shell length (sl), base shell (bs), shell height (sh) and the angle detachment (θ) for each individual. Thus, it was possible to develop Equations (1)–(4) (new equations). From these data, using the Excel spreadsheet, we obtained a curve that relates the angle "θ" with the "sl" and then adjusted Equation (1), which had a coefficient $R^2 = 0.9935$. It was observed by measuring GM husks that the dimension formed between the vertex of the triangle and the top of the bark has a constant ratio of "0.76 · sl" (Figure 4). Thus, it was obtained from trigonometric relation Equation (2), which provides the dimension "sh". Dimension "bs," also obtained by measuring GM shells, corresponds to 38% of shell length "sh" and can be calculated by Equation (3). The "e" corresponds to 62% of the dimension "sh" and can be calculated by Equation (4).

$$\theta = 29.989 \cdot sl^{0.0951} \quad (1)$$

$$sh = 0.760 \cdot sl \cdot \tan\theta \quad (2)$$

$$bs = 0.288 \cdot sl \cdot \tan\theta \quad (3)$$

$$e = 0.472 \cdot sl \cdot \tan\theta \quad (4)$$

sl: shell length (mm);
θ: attachment angle (degree);
sh: shell height (mm)
bs: shell base (mm);
e: roughness (mm).

The criteria to determine the thickness of the biofouling were created based on the roughness (Equation (4)) of the surface and calculated without considering the hydrodynamic drag detachment of specimens from the pumping system. This detachment, in turn, was derived from the decrease in the free flow diameter, which was caused by the thickness

of the biofouling and the elevation in the velocity flow in the pipe. Thus, using Equation (4), it was possible to determine a characteristic roughness curve as a function of bioinfestation time, allowing for the evaluation of the new flow-free diameters.

### *2.5. Mathematical Analysis: Calculation of the Thickness of the Biofouling in Pipelines of Average Roughness*

With the determination of the shell height using Equation (2), it was possible to calculate the thickness of the biofouling, according to the hydrodynamic drag detachment. However, it is important to consider the interference of flow velocity in the progression of biofouling in pipelines. Based on the studies of Castro (2013) [45], it is assumed that the velocity effect gradually increased the detachment of the mussels. A detachment of 20% of the thickness of the biofouling is seen between the speed ranges 2.0 m/s and 2.5 m/s. Thereafter, a detachment of 40% is found between 3.0 m/s and 3.5 m/s, advancing to 60% between 3.5 m/s and 4.0 m/s, and to up to 80% at velocities above 4.0 m/s. When the velocity reaches 4.5 m/s, all new specimens become detached.

Based on the information above, the thickness of the biofouling was calculated related to percentage of detachment, after the beginning of the formation of the second layer of the GM (Equation (5)).

$$bt = sh + sh^{*}(1 - \%_{detachment.})_{1^{a}layer} + sh^{*}(1 - \%_{detachment.})_{2^{a}layer} + \ldots sh^{*}(1 - \%_{detachment.})_{n^{a}layer} \quad (5)$$

bt: thickness of the biofouling;

$\%_{dettachment}$: percentage of detachment of the GM.

We assume that, once the value of the thickness of the biofouling exceeds the value of the average roughness of the surface, the second layer of biofouling starts to form.

This creates a pattern for the growth of the layers and makes it possible to estimate the thickness of the biofouling for any time period of infestation. It should be considered that the growth of the GM is not uniform and that the colonies have specimens of various sizes. This leads the average roughness to be affected by the diversity of these specimens.

The parameter chosen to obtain the roughness caused by biofouling was the average roughness ($R_a$), which is a parameter applied in most engineering processes [46,47]. To determine the Ra using Equation (6), photographs of the surfaces (ASTM-A36 steel) with artificially attached dried shells were used (see Section 2.4). On each surface (nine), a midline was drawn (from the mussel fixation base), through which measurements were made between peaks and valleys, as described in Han et al. (2019) [48].

$$R_a = \frac{1}{n}\sum_{i=1}^{n}|e_i| \ (mm) \quad (6)$$

$R_a$: average roughness (mm);

n: number of measurements taken;

### *2.6. Load Loss*

Since biofouling occurred on the entire inner surface of the pipe, the free flow diameter (D) in the pipe was decreased by twice the value of the thickness of the biofouling.

The velocity flow inside the pipes was obtained from the data of the EPS studied [36]. The reduction of the diameter was based on the thickness of the biofouling and was calculated by using the equation of continuity, Equation (7) [49].

$$V = \frac{Q}{A} \quad (7)$$

Q: flow rate ($m^3/s$);

A: area of the pipeline ($m^2$).

In order to calculate the load loss factor ($f$), a function was defined, using Equation (8), Buzzelli's Equation [50]. This equation contains two roots: $B_1$ obtained using Equation (9),

and $B_2$ Equation (10), obtained as a function of $R_a$ (average roughness), D (free flow diameter), and the Reynolds number (Re), which was obtained from Equation (11) [49]. All calculations were carried out considering two scenarios: a pumping system without biofouling and a pumping system with biofouling. The value of the roughness of the pipe surface (ASTM-A36 steel), was considered as $e = 0.045$mm [17], which was the value considered for the system without biofouling.

$$\frac{1}{\sqrt{f}} = B_1 - \left( \frac{B_1 + 2 \cdot \log_{10}\left(\frac{B_2}{Re}\right)}{1 + \frac{2.18}{B_2}} \right) \tag{8}$$

$$B_1 = \frac{(0.777 \cdot \ln \cdot (Re)) - 1.41}{1 + 1.32\sqrt{\frac{R_a}{D}}} \tag{9}$$

$$B_2 = \frac{R_a}{3.7 \cdot D} \cdot Re + 2.51 \cdot B_1 \tag{10}$$

$$Re = \frac{V \cdot D}{\gamma} \tag{11}$$

$f$: load loss factor;
$B_1$: root 1;
$B_2$: root 2;
Re: Reynolds number;
D: free flow diameter (m);
$\gamma$: kinematic viscosity of water, $10^{-6}$ $\left(m^2/s\right)$.

With the values obtained above, the load loss was calculated using the Darcy–Weisbach equation, Equation (12) [51].

$$\Delta H = \frac{8 \cdot f \cdot Q^2 \cdot L}{\pi^2 \cdot g \cdot D^5} \tag{12}$$

$\Delta H$: load loss (mca);
L: pipe length (m);
g: gravity acceleration —9.81 $\left(m/s^2\right)$.

To determine the total height of the elevation, or the total load loss of the pumping system, Equation (13) was used [51].

$$H_{total} = H_{gh} + \Delta H_{head} \tag{13}$$

$H_{total}$: total height of the elevation (mca);
$H_{gh}$: the average geometric gradient to be compensated for (mca);
$\Delta H_{head}$: sum of the load loss due to suction and the discharge pipe (mca).

The load loss due to suction and the discharge pipe was calculated using Equation (14) [51].

$$\Delta H_{head} = \frac{8 \cdot f \cdot Q^2 \cdot L_{discharge}}{\pi^2 \cdot g \cdot \left(D_{discharge}\right)^5} + \frac{8 \cdot f \cdot Q^2 \cdot L_{suction}}{\pi^2 \cdot g \cdot \left(D_{suction}\right)^5} \tag{14}$$

The methodology used here to calculate the load loss was also described by Mataix (2009) [49].

### *2.7. Energy Efficiency*

The pumping power needs to be known for the calculation of the economic cost of pumping. Equation (15) [51], shown below, considers the yield of the pumps as described by Mataix (2009) [49] and the water working fluid at atmospheric pressure.

$$P_{kW} = \frac{(\gamma \cdot Q \cdot H_{total})}{\eta \cdot 1000} \tag{15}$$

P: pumping power (kW);
$\gamma$: water-specific weight (kgf/m$^3$);
$\eta$: efficiency.

The consumption, of the pumping system without bioinfestation, taking into account the potency obtained for said system was obtained using Equation (16) [49].

$$C_{\text{without inf}} = P_{\text{without inf}} \cdot \sum_{1}^{n} t_{\text{op.}} \quad (16)$$

$C_{\text{without inf}}$ : consumption of the pumping system without bioinfestation (kWh);
$P_{\text{without inf}}$: power calculated for the pumping system without bioinfestation (kW);
$t_{\text{op.}}$: number of operating hours of the pumping system in hours, days, or years.

The consumption of the pumping system with bioinfestation, taking into account the potency obtained for said system, was obtained using Equation (17), [49].

$$C_{\text{inf}} = P_{\text{inf}} \cdot \sum_{1}^{n} t_{\text{op.}} \quad (17)$$

$C_{\text{inf}}$ : consumption of the pumping system with bioinfestation (kWh);
$P_{\text{inf}}$: power calculated for the pumping system with bioinfestation.

The increase in energy consumption by hour is the value of the difference in power between the systems with and without biofouling, multiplied by the pumping operation time. This calculation is given as Equation (18) (improved equation) [49].

$$C_{\text{inf}} = (P_{\text{inf}} - P_{\text{without inf}}) \cdot \sum_{1}^{n} t_{\text{op.}} \quad (18)$$

The costs of the pumping system per cubic meter without bioinfestation were obtained via Equation (19) [49], in view of the consumption of the pumping system and of the volume that was pumped.

$$C_{\text{pumping without inf.}} = \frac{C_{\text{without inf.}}}{V_{\text{pumping}}} \cdot \text{Price} \quad (19)$$

$C_{\text{pumping without inf.}}$ : cost of pumping per cubic meter before infestation (USD/m$^3$);
$V_{\text{pumping}}$: volume that was pumped (m$^3$);
Price: price per kWh (USD/kWh).

The cost of the pumping system per cubic meter with bioinfestation was obtained by using Equation (20) [49], in view of the consumption of the pumping system with bioinfestation and of the volume that was pumped.

$$C_{\text{pumping inf.}} = \frac{C_{\text{inf.}}}{V_{\text{pumping}}} \cdot \text{Price} \quad (20)$$

$C_{\text{pumping inf.}}$: cost of pumping per cubic meter after bioinfestation (USD/m$^3$).

## 3. Results and Discussion

### *3.1. Shell Growth, Thickness of Biofouling and Roughness of the Surface*

One of the main challenges of the present work when linked to the loss of energetic efficiency, pumping system, and the golden mussel (GM) was to obtain the growth curve based on the data presented in Table 3. The results allow, through this biological information, the construction of new equations and the improvement of others, allowing for an analysis of the loss of energy efficiency.

The measurements (see Figure 4) and the proportionality relationship among the measured individuals obtained using Equations (1) and (4) allow the determination of

the temporal curve of surface roughness. The calculation of the biofouling thickness was conducted using Equations (2), (3) and (5). The analysis of the three parameters (GM growth curve, temporal curve of roughness, and biofouling thickness) is shown in Figure 5.

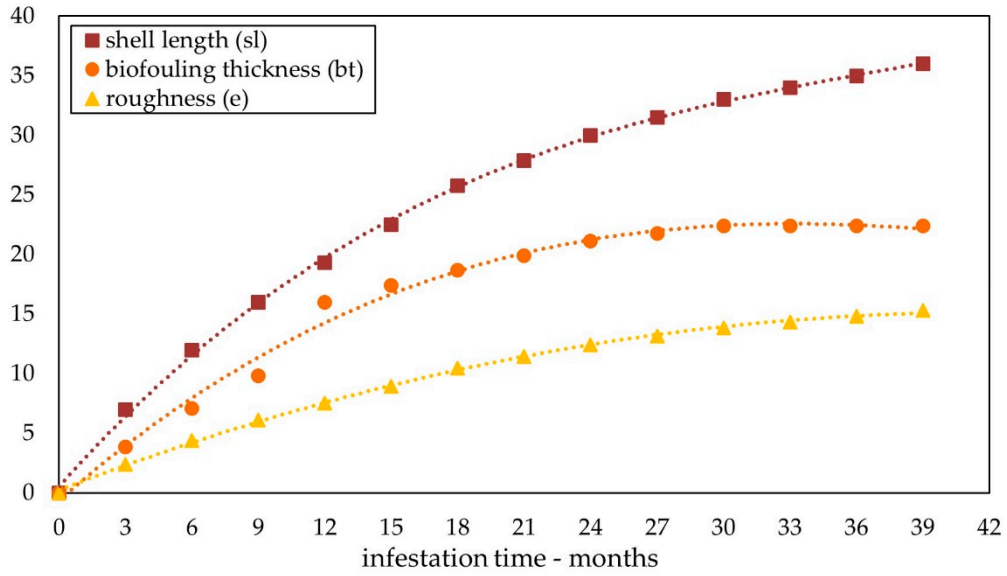


**Figure 5.** Golden mussel growth curve based on shell length (sl), average thickness of biofouling (bt), and surface roughness (e). All data are related to time and were obtained from Table 3.

Figure 5 shows that in the first year of bioinfestation (0–12 months), the shell length reached 20 mm, showing exponential growth. In the second year of bioinfestation (12–24 months), the GM grew only 10 mm, showing that there was a 50% reduction in the growth rate when compared with the first year. This behavior is also verified in the third year of bioinfestation (24–36 months), where a shell length growth of 5 mm was observed for this period, which also showed a 50% reduction in the growth rate when compared with the previous year. This growth dynamic, shown in the graph prepared from literature data (Table 3), showed that there is a stabilization trend in growth as the GM approaches its maximum size (35–40 mm). These data are in agreement with those of Darrigran and Maroñas (2002) [40], who show a trend towards stabilization after a period of 3 years, when the shell length reaches its maximum.

The characteristic roughness curve (Figure 5) shows an average growth rate of approximately 65% for the period from 0 to 18 months of bioinfestation, coinciding with the average value of surface roughness calculated through Equation (6) (see Section 2.5), which was $R_a = 10.25$ mm. This roughness was used to determine the beginning of the formation of the second biofouling layer and to calculate the load loss. After this period (18–33 months), the average growth rate fell approximately 25%, demonstrating that the increase in shell length does not directly influence the increase in roughness. After 33 months of bioinfestation, it was found that the curve tends to stabilize.

According to Burlakova et al. (2022) [18], *Dreissena* spp. (zebra mussel) and *Limnoperna fortunei* (GM) have similar life histories and share functional ecological characteristics, in addition to having a byssus that allows attachment to various substrates. It is also known that the zebra mussel causes an increase in surface roughness after the beginning of bioinfestation, and that densities of 32 ind/cm$^2$ have already been detected [30]. Therefore, these characteristics provide a warning with regard to the issue of increasing GM population density, which would contribute to an increase in roughness.

After 15 months of bioinfestation (Figure 5), the layer thickness presented a value of approximately 17 mm, corresponding to an average growth rate of 1.1 mm/month. For the subsequent period (15–27 months), the average growth progression of the biofouling thickness fell to 0.3 mm/month. This reduction was due to the increase in the hydrody-

namic drag detachment, which varies depending on the speed, calculated by Equation (7), inhibiting the progression of the colonies because of the detachment of new specimens, as also observed by Simeão (2011) [44], Castro (2013) [45], and Xu et al. (2012) [52].

The importance of pumping systems in energy production, and indeed, the whole issue of biofouling and its interference, especially in terms of roughness, is well-known, being able to affect the efficiency of the system. In addition, it is also known from records in the literature that the GM can affects ecosystem services related to human well-being and is associated with ecosystem disservices (e.g., biofouling, toxic cyanobacterial bloom, and transfer of contaminants) [18].

### *3.2. Load Loss Factor and Free Flow Diameter*

After determining the layer thickness, it is possible to determine the free flow diameter (see Section 2.6), taking into account its reduction caused by the increase in the thickness of the biofouling. The values of f were calculated for the pumping system analysed in our case study and two situations were considered: the system without biofouling and with biofouling. Figure 6 shows the curves of the progression of f along with the reduction in the diameters of the pipes coupled to pumps 1, 2, and 3, at the Rio Branco EPS.

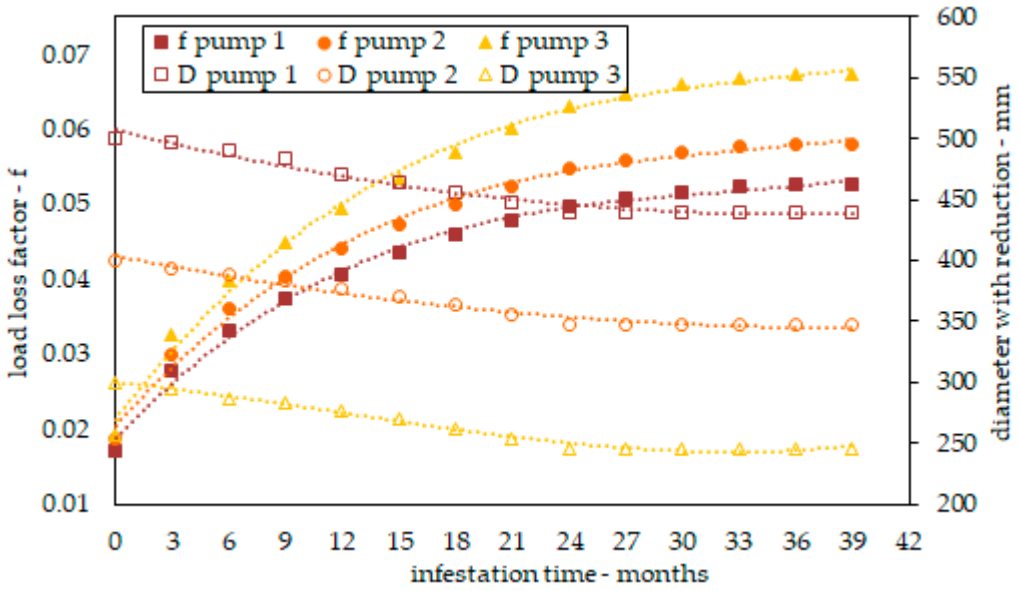


**Figure 6.** Temporal progression of the load loss factor (f) of the pumping system, calculated using Equation (8) and the reduction in the free flow diameter (D) due to biofouling, for the pumping systems coupled to pumps 1 (B1), 2 (B2) and 3 (B3). Data are presented in Table 1.

To construct these curves, it was necessary to calculate the load loss factors ($f$), using Equations (8)–(11). All of these equations were used in the two systems evaluated: with and without biofouling. The values of $f$ for the pipes attached to the pumps without the occurrence of bioinfestation were as follows: Pump 1: $f$ = 0.01710; Pump 2: $f$ = 0.01874; and Pump 3: $f$ = 0.01933.

The construction of the $f$ curve took into account as the first value the load loss factor of the pumping system without biofouling and from that point on, the calculations were made by taking into account the decrease in free flow diameter, caused by the increase in the thickness of the biofouling, as shown in Figure 5. The $f$ curve for Pump 1 presents an average increase over 3 years (0–36 months) of 207%, compared with the $f$ value for the system without biofouling. It can be seen that this value is even more pronounced for Pumps 2 and 3, with average increases for the same period of 209% and 248%, respectively. This proves the theory that the efficiency of the system decreases as the load loss factor increases [29].

The curves have the same characteristic of entering stability close to 24 months of bioinfestation, decreasing the growth rate of *f*. This may be caused by several factors, including: (i) variation in the shell growth and drag force on the GM; (ii) the death of specimens that subsequently detach from the surface; and (iii) the detachment of parts of the colony as a result of the degradation of the dead specimens that are inserted in the first layers of encrustation. It is important to note that the initial velocity flows in these pipes are not equal, and only equalize after the stabilization of the biofouling.

As the velocity flow increases, an increase in the detachment rate follows, causing a decrease in the thickness of the biofouling. It is known that the longer the shell length, the greater the attachment force, making it more difficult to remove shells in terms of the velocity factor [52], although it is already proven that the increase in velocity inside the pipe causes the pullout of individuals, especially in steel [45]. Until the beginning of the formation of the second layer, the thickness of the biofouling for both the pumping system with and without bioinfestation is considered equal. After one year of bioinfestation, with the layer thickness having reached the value of average roughness and including the effect of increased velocity, hydrodynamic drag detachment was considered. It is assumed that the lower layers will not progress after a subsequent layer begins to form, as they will not have access to filtration, and will become substrates for future specimens. This can be seen in Figure 6.

The effect of the detachment of the specimens after bioinfestation is stabilized has the potential to damage the pumps as it can increase the wear of the impeller, the sealing systems, and the seals, as a result of friction from the GM shell [35].

### *3.3. Energy Consumption Costs of Pumping System with Biofouling*

Although the loss of energy efficiency is a broad topic, only a few parameters were selected for this study, such as energy consumption and cost of pumping, which allowed for the analysis of the loss of energy efficiency/pumping system due to the GM. This issue is admitted in the analysis of industrial sectors, but has not been scientifically analyzed or published in a robust and reliable way.

Here, to determine the cost of pumping per $m^3$, which, together with energy consumption, determined the efficiency of the pumping system, it was necessary to calculate the energy consumption using Equations (12)–(17). For these calculations, the two scenarios of the target pumping system were considered: with biofouling and without biofouling. The results of Equations (12)–(17) pointed to the greater load loss, power, and energy consumption of systems with biofouling (Tables 4–7).

The energy consumption values of the pipelines coupled to Pumps 1, 2, and 3 (in the scenario without biofouling; Equation (16)) were determined as 110 kWh, 60 kWh, and 39 kWh, respectively, for the scenario with biofouling, and are also given in the tables cited. Figure 7 shows the increase in energy consumption in kWh for the two systems evaluated, calculated using Equation (18) for each pipe coupled to Pumps 1, 2, and 3.

As the pumping system undergoes the beginning of bioinfestation, there is an increase in the energy consumption required to maintain the flow at the same level as in the system without biofouling. This demand causes an increase in the pumping consumption, as presented through the curves, for each system coupled to Pumps 1, 2, and 3 (Figure 7).

At the end of two years (0–24 months) of bioinfestation, there were increases in the consumption of 34%, 30%, and 95% for Pumps 1, 2, and 3, respectively. After this period (24–39), consumption tends to enter stability, reaching an increase of 36%, 32%, and 102% by the end of the period for the coupled systems of Pumps 1, 2, and 3, respectively. With this information, it was found that the growth rate of consumption is higher in the first 24 months, proving the relationship with the increase in the load loss factor (Figure 6).

**Table 4.** Progression of consumption and costs, in view of the progression of GM bioinfestation for Pump 1, with a flow rate of 600 L/s and a diameter of 500 mm.

| Month | $s_h$ | D | Q | *f* | ΔH | $H_{total}$ | | $D_{vd}$ | $P_{pump}$ | $T_{ab}$ | C1 | C2 | C3 | C4 | C5. | C6. | C7. | Incr. |
|---|---|---|---|---|---|---|---|---|---|---|---|---|---|---|---|---|---|---|
| 0 | 0.0 | 500.0 | 600.0 | 0.0171 | 1.2 | 14.6 | 78.3 | 0.0 | 109.9 | 0.0 | 1318 | 118,663 | - | 0.00 | 171.40 | 15,426.00 | 0.0066 | - |
| 3 | 3.9 | 496.9 | 596.0 | 0.0278 | 1.9 | 15.4 | 78.3 | 173.0 | 114.9 | 0.1 | 1388 | 124,887 | 6224 | 809.10 | 180.39 | 16,235.00 | 0.0070 | 5% |
| 6 | 7.1 | 491.2 | 595.0 | 0.0333 | 2.4 | 15.9 | 78.3 | 216.0 | 118.4 | 0.1 | 1433 | 128,985 | 10,321 | 1341.78 | 186.31 | 16,768.00 | 0.0072 | 9% |
| 9 | 9.8 | 483.4 | 593.0 | 0.0373 | 2.9 | 16.4 | 78.3 | 302.0 | 121.8 | 0.1 | 1479 | 133,101 | 14,438 | 1876.97 | 192.26 | 17,303.00 | 0.0074 | 12% |
| 12 | 16.0 | 470.6 | 592.0 | 0.0408 | 3.7 | 17.1 | 78.3 | 346.0 | 126.9 | 0.2 | 1544 | 138,938 | 20,274 | 2635.68 | 200.69 | 18,062.00 | 0.0077 | 17% |
| 15 | 17.4 | 463.6 | 591.0 | 0.0435 | 4.2 | 17.6 | 78.3 | 389.0 | 130.7 | 0.2 | 1592 | 143,294 | 24,631 | 3201.98 | 206.98 | 18,628.00 | 0.0080 | 21% |
| 18 | 18.7 | 456.2 | 589.0 | 0.0459 | 4.8 | 18.2 | 78.3 | 475.0 | 134.5 | 0.2 | 1644 | 147,933 | 29,269 | 3805.02 | 213.68 | 19,231.00 | 0.0082 | 25% |
| 21 | 19.9 | 448.2 | 587.0 | 0.0479 | 5.4 | 18.8 | 78.2 | 562.0 | 138.7 | 0.3 | 1701 | 153,097 | 34,434 | 4476.39 | 221.14 | 19,903.00 | 0.0085 | 29% |
| 24 | 21.2 | 439.7 | 584.0 | 0.0497 | 6.1 | 19.5 | 78.2 | 691.0 | 143.0 | 0.3 | 1762 | 158,617 | 39,954 | 5194.05 | 229.11 | 20,620.00 | 0.0088 | 34% |
| 27 | 21.8 | 439.7 | 584.0 | 0.0509 | 6.2 | 19.7 | 78.2 | 691.0 | 144.1 | 0.3 | 1777 | 159,918 | 41,255 | 5363.12 | 230.99 | 20,789.00 | 0.0089 | 35% |
| 30 | 22.4 | 439.7 | 584.0 | 0.0517 | 6.3 | 19.8 | 78.2 | 691.0 | 144.9 | 0.3 | 1786 | 160,769 | 42,105 | 5473.71 | 232.22 | 20,900.00 | 0.0090 | 35% |
| 33 | 22.4 | 439.7 | 584.0 | 0.0523 | 6.4 | 19.9 | 78.2 | 691,0 | 145.4 | 0.3 | 1793 | 161,353 | 42,690 | 5549.70 | 233.07 | 20,976.00 | 0.0090 | 36% |
| 36 | 22.4 | 439.7 | 584.0 | 0.0526 | 6.4 | 19.9 | 78.2 | 691.0 | 145.7 | 0.3 | 1796 | 161,681 | 43,018 | 5592.29 | 233.54 | 21,018.00 | 0.0090 | 36% |
| 39 | 22.4 | 439.7 | 584.0 | 0.0527 | 6.5 | 19.9 | 78.2 | 691.0 | 145.8 | 0.3 | 1797 | 161,756 | 43,093 | 5602.10 | 233.65 | 21,028.00 | 0.0090 | 36% |

The meanings of the symbols are as follows: $s_h$, thickness of the biofouling—mm; D, effective diameter—mm; Q, flow—L/s; *f*, load loss factor; ΔH, load loss—mca; $H_{total}$, total height of elevation—mca; $\eta$, efficiency—%; $D_{vd}$, daily flow deficit—$m^3$; $P_{pump}$, power of the pump—kW; $T_{ab}$, additional pumping time—h/day; C1, pumping system consumption—kWh/day; C2, pumping system consumption—kWh/trimester; C3, incremental consumption—kWh/trimester; C4, incremental costs—US$/trimester; C5, daily costs—USD/day; C6, total cost per trimester—USD; C7, pumping cost—$m^3$); and Incr., increased consumption.

**Table 5.** Progression of consumption and costs, in view of the progression of GM bioinfestation for Pump 2, with a flow rate of 300 L/s and a diameter of 400 mm.

| Month | $s_h$ | D | Q | *f* | ΔH | $H_{total}$ | | $D_{vd}$ | $P_{pump}$ | $T_{ab}$ | C1 | C2 | C3 | C4 | C5. | C6. | C7. | Incr. |
|---|---|---|---|---|---|---|---|---|---|---|---|---|---|---|---|---|---|---|
| 0 | 0.0 | 400 | 300.0 | 0.0187 | 1.0 | 14.4 | 70.7 | 0.0 | 60.1 | 0.0 | 721 | 64,927 | 0 | 0.00 | 93.78 | 8440.00 | 0.0072 | - |
| 3 | 3.9 | 394 | 293.5 | 0.0300 | 1.7 | 15.2 | 71.3 | 280.8 | 61.3 | 0.3 | 752 | 67,669 | 2743 | 356.53 | 97.74 | 8797.00 | 0.0075 | 4% |
| 6 | 7.1 | 388 | 288.5 | 0.0360 | 2.2 | 15.7 | 71.6 | 496,8 | 61.9 | 0.5 | 773 | 69,528 | 4601 | 598.09 | 100.43 | 9039.00 | 0.0077 | 7% |
| 9 | 9.8 | 384 | 285.0 | 0.0405 | 2.6 | 16.1 | 71.9 | 648.0 | 62.5 | 0.6 | 790 | 71,080 | 6153 | 799.93 | 102.67 | 9240.00 | 0.0079 | 9% |
| 12 | 16.0 | 378 | 282.0 | 0.0442 | 3.1 | 16.6 | 72.1 | 777.6 | 63.6 | 0.8 | 812 | 73,051 | 8124 | 1056.10 | 105.52 | 9497.00 | 0.0081 | 13% |

**Table 5.** *Cont.*

| Month | $s_{ht}$ | D | Q | *f* | ΔH | $H_{total}$ | | $D_{vd}$ | $P_{pump}$ | $T_{ab}$ | C1 | C2 | C3 | C4 | C5. | C6. | C7. | Incr. |
|---|---|---|---|---|---|---|---|---|---|---|---|---|---|---|---|---|---|---|
| 15 | 17.4 | 371 | 279.0 | 0.0474 | 3.7 | 17.1 | 72,3 | 907.2 | 64.8 | 0.9 | 836 | 75,282 | 10,355 | 1346.15 | 108.74 | 9787.00 | 0.0084 | 16% |
| 18 | 18.7 | 363 | 277.0 | 0.0501 | 4.3 | 17.7 | 72.4 | 993.6 | 66.6 | 1.0 | 866 | 77,920 | 12,993 | 1689.09 | 112.55 | 10,130.00 | 0.0087 | 20% |
| 21 | 19.9 | 355 | 276.0 | 0.0525 | 5.0 | 18.5 | 72.4 | 1036.8 | 69.1 | 1.0 | 901 | 81,084 | 16,158 | 2100.48 | 117.12 | 10,541.00 | 0.090 | 25% |
| 24 | 21.2 | 347 | 270.0 | 0.0547 | 5.9 | 19.4 | 72.7 | 1296.0 | 70.5 | 1.3 | 940 | 84,571 | 19,644 | 2553.75 | 122.16 | 10,994.00 | 0.0094 | 30% |
| 27 | 21.8 | 347 | 269.0 | 0.0560 | 6.0 | 19.5 | 72.8 | 1339.2 | 70.7 | 1.4 | 946 | 85,571 | 20,208 | 2626.98 | 122.97 | 11,067.00 | 0.0095 | 31% |
| 30 | 22.4 | 347 | 269.0 | 0.0570 | 6.2 | 19.6 | 72.8 | 1339.2 | 71.1 | 1.4 | 951 | 85,598 | 20,671 | 2687.29 | 123.64 | 11,128.00 | 0.0095 | 32% |
| 33 | 22.4 | 347 | 269.0 | 0.0577 | 6.2 | 19.7 | 72.8 | 1339.2 | 71.3 | 1.4 | 955 | 85,917 | 20,991 | 2728.78 | 124.10 | 11,169.00 | 0.0096 | 32% |
| 36 | 22.4 | 347 | 269.0 | 0.0580 | 6.3 | 19.7 | 72.8 | 1339.2 | 71.5 | 1.4 | 957 | 86,096 | 21,170 | 2752.04 | 124.36 | 11,193.00 | 0.0096 | 33% |
| 39 | 22.4 | 347 | 269.0 | 0.0581 | 6.3 | 19.7 | 72.8 | 1339.2 | 71.5 | 1.4 | 957 | 86,138 | 21,211 | 2757.40 | 124.42 | 11,198.00 | 0.0096 | 33% |

The meanings of the symbols are as follows: $s_{ht}$, thickness of the biofouling—mm; D, effective diameter—mm; Q, flow—L/s; *f*, load loss factor; ΔH, load loss—mca; $H_{total}$, total height of elevation—mca; $\eta$, efficiency—%; $D_{vd}$, daily flow deficit—$m^3$; $P_{pump}$, power of the pump—kW; $T_{ab}$, additional pumping time—h/day; C1, pumping system consumption—kWh/day; C2, pumping system consumption—kWh/trimester; C3, incremental consumption—kWh/trimester; C4, incremental costs—US$/trimester; C5, daily costs—USD/day; C6, total cost per trimester—USD; C7, pumping cost—$m^3$); and Incr., increased consumption.

**Table 6.** Progression of consumption and costs, in view of the progression of GM bioinfestation for Pump 3, with a flow rate of 200 L/s and a diameter of 300 mm.

| Month | $s_{ht}$ | D | Q | *f* | ΔH | $H_{total}$ | | $D_{vd}$ | $P_{pump}$ | $T_{ab}$ | C1 | C2 | C3 | C4 | C5. | C6. | C7. | Incr. |
|---|---|---|---|---|---|---|---|---|---|---|---|---|---|---|---|---|---|---|
| 0 | 0.0 | 300 | 200.0 | 0.0193 | 1.9 | 15.3 | 77.4 | 0.0 | 38.9 | 0.0 | 466.9 | 42,017 | 0 | 0 | 60.69 | 5462.21 | 0.0070 | 0 |
| 3 | 3.9 | 295 | 199.0 | 0.0325 | 3.4 | 16.9 | 77.5 | 43.2 | 42.6 | 0.1 | 513.5 | 46,215 | 4198 | 545,69 | 66.75 | 6007.90 | 0.0077 | 10% |
| 6 | 7.1 | 287 | 197.0 | 0.0397 | 4.9 | 18.3 | 77.6 | 129.6 | 45.6 | 0.2 | 555.5 | 49,998 | 7981 | 1037.57 | 72.22 | 6499.78 | 0.0084 | 19% |
| 9 | 9.8 | 283 | 195.0 | 0.0450 | 5.9 | 19.4 | 77.8 | 216.0 | 47.6 | 0.3 | 586.2 | 52,756 | 10,739 | 1396.08 | 76.20 | 6858.29 | 0.0088 | 26% |
| 12 | 16.0 | 277 | 193.0 | 0.0496 | 7.3 | 20.7 | 77.9 | 302.4 | 50.4 | 0.4 | 627.0 | 56,429 | 14,412 | 1873.62 | 81.51 | 7335.83 | 0.0094 | 34% |
| 15 | 17.4 | 270 | 191.0 | 0.0535 | 8.9 | 22.4 | 78.0 | 388.8 | 53.8 | 0.6 | 676.0 | 60,844 | 18,827 | 2447.49 | 87.89 | 7909.70 | 0.0102 | 45% |
| 18 | 18.7 | 262 | 189.0 | 0.0570 | 11.0 | 24.4 | 78.1 | 475.2 | 58.0 | 0.7 | 736.4 | 66,277 | 24,260 | 3153.82 | 95.73 | 8616.02 | 0.0111 | 58% |
| 21 | 19.9 | 254 | 188.0 | 0.0602 | 13.5 | 27.0 | 78.1 | 518.4 | 63.7 | 0.8 | 812.8 | 73,152 | 31,135 | 4047.55 | 105.66 | 9509.76 | 0.0122 | 74% |
| 24 | 21.2 | 246 | 180.0 | 0.0631 | 16.8 | 30.2 | 78.2 | 864.0 | 68.3 | 1.3 | 910.3 | 81,923 | 39,906 | 5187.80 | 118.33 | 10,650.01 | 0.0137 | 95% |
| 27 | 21.8 | 246 | 179.0 | 0.0648 | 17.2 | 30.7 | 78.2 | 907.2 | 68.9 | 1.4 | 923.5 | 83,111 | 41,094 | 5342.23 | 120.05 | 10,804.43 | 0.0139 | 98% |

**Table 6.** *Cont.*

| Month | $s_h$ | D | Q | *f* | ΔH | $H_{total}$ | | $D_{vd}$ | $P_{pump}$ | $T_{ab}$ | C1 | C2 | C3 | C4 | C5. | C6. | C7. | Incr. |
|---|---|---|---|---|---|---|---|---|---|---|---|---|---|---|---|---|---|---|
| 30 | 22.4 | 246 | 179.0 | 0.0660 | 17.5 | 31.0 | 78.2 | 907.2 | 69.6 | 1.4 | 933.3 | 83,998 | 41,981 | 5457.54 | 121.33 | 10,919.75 | 0.0140 | 100% |
| 33 | 22.4 | 246 | 179.0 | 0.0668 | 17.8 | 31.2 | 78.2 | 907.2 | 70.1 | 1.4 | 940.1 | 84,609 | 42,592 | 5536.99 | 122.21 | 10,999.19 | 0.0141 | 101% |
| 36 | 22.4 | 246 | 179.0 | 0.0673 | 17.9 | 31.3 | 78.2 | 907.2 | 70.4 | 1.4 | 943.9 | 84,952 | 42,935 | 5581.58 | 122.71 | 11,043.79 | 0.0142 | 102% |
| 39 | 22.4 | 246 | 179.0 | 0.0674 | 17.9 | 31.4 | 78.2 | 907.2 | 70.5 | 1.4 | 944.8 | 85,031 | 43,014 | 5591.87 | 122.82 | 11,054.07 | 0.0142 | 102% |

The meanings of the symbols are as follows: $s_h$, thickness of the biofouling—mm; D, effective diameter—mm; Q, flow—L/s; *f*, load loss factor; ΔH, load loss—mca; $H_{total}$, total height of elevation—mca; η, efficiency—%; $D_{vd}$, daily flow deficit—$m^3$, power of the pump—kW; $T_{ab}$, additional pumping time—h/day; C1, pumping system consumption—kWh/day; C2, pumping system consumption—kWh/trimester; C3, incremental consumption—kWh/trimester; C4, incremental costs—US$/trimester; C5, daily costs—USD/day; C6, total cost per trimester—USD; C7, pumping cost—$m^3$); and Incr., increased consumption.

**Table 7.** Summary of the impact of GM bioinfestation at Rio Branco EPS until the period of stabilization.

| | Daily Consumption (kWh/Day) | Daily Cost (USD/Day) | Increase (USD/Day) | Cost Per Unit (USD·$M^3$) | Increase (USD/$M^3$) | Increase in Consumption (%) |
|---|---|---|---|---|---|---|
| year | 2.506.7 | 325.88 | - | 0.00686 | - | - |
| 1 year | 2982.4 | 387.71 | 61.84 | 0.00816 | 0.00130 | 19 |
| 2 years | 3612.5 | 469.62 | 143.74 | 0.00988 | 0.00302 | 44 |
| 2.5 years | 3.670.7 | 447.19 | 151.32 | 0.01004 | 0.00318 | 46 |

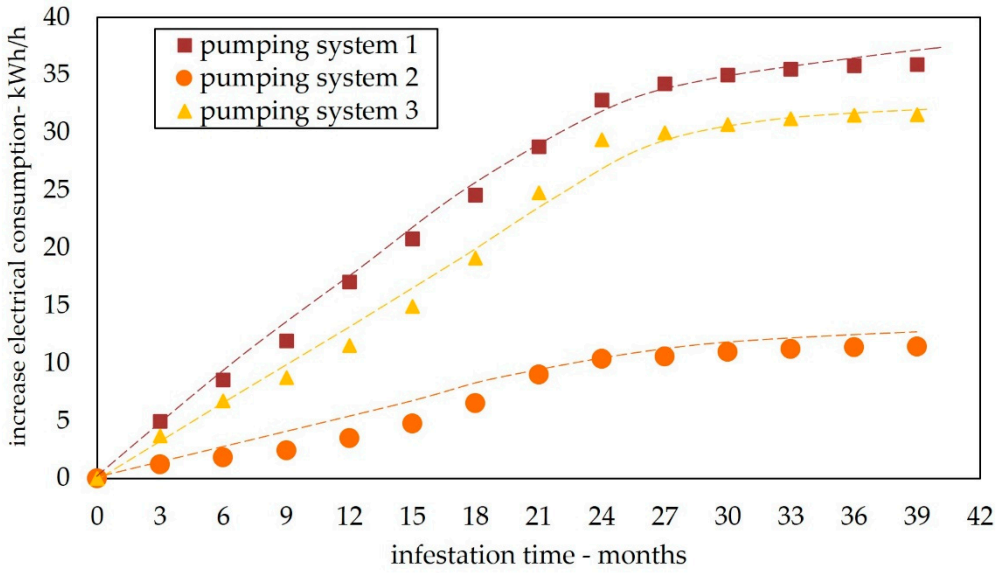


**Figure 7.** Increase in consumption in kilowatt hours (kWh) for each pump of the Elevated Pumping Station (EPS) of Rio Branco, after the beginning of the golden mussel (GM) bioinfestation, based on the data from Tables 4–6, and in view of the operating time, given in months.

Figure 8 shows the curve for the total daily consumption of the system with biofouling, considering operation for 12 h.

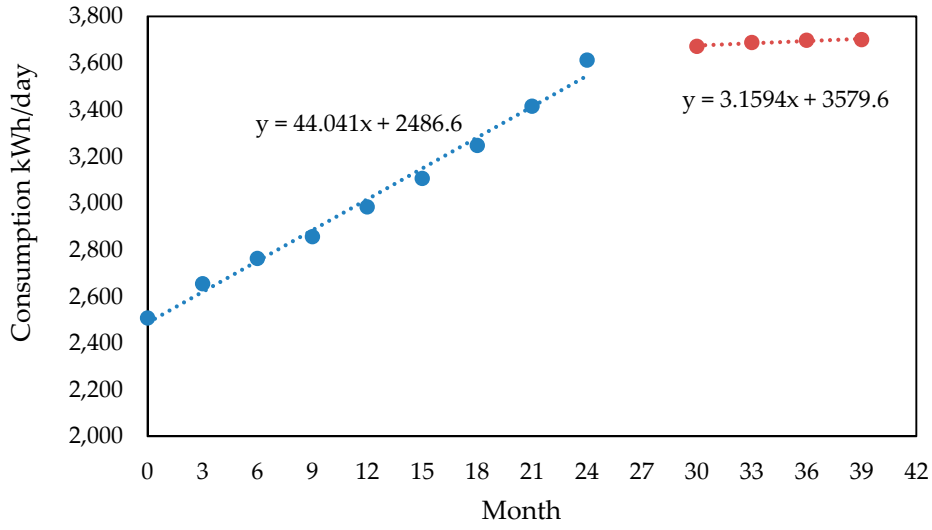


**Figure 8.** Total daily consumption rate of the Elevated Pumping System of Rio Branco, considering biofouling.

When analyzing the growth rate of the segregated bioinfestation in two different periods (0–24 and 27–30 months), it is possible to conclude that the growth rate of consumption is constant for the first 24 months. After this period, saturation of growth occurs and, the rate of loss is enhanced by the rate of detachment, which leads to a second period of equilibrium (30–39 months). The progression rate is noted to drop to close to 10% of the initial value (Figure 8).

After determining the consumption, it is possible to determine the cost of pumping per $m^3$, knowing the price per kWh in the Acre State region to be USD 0.13 [53,54]. Using Equations (19) and (20), we can calculate the cost of pumping for the system without biofouling and with biofouling, respectively. Figure 9 shows the relationship between

energy consumption and cost of pumping, evaluating the two scenarios dealt with in this work.

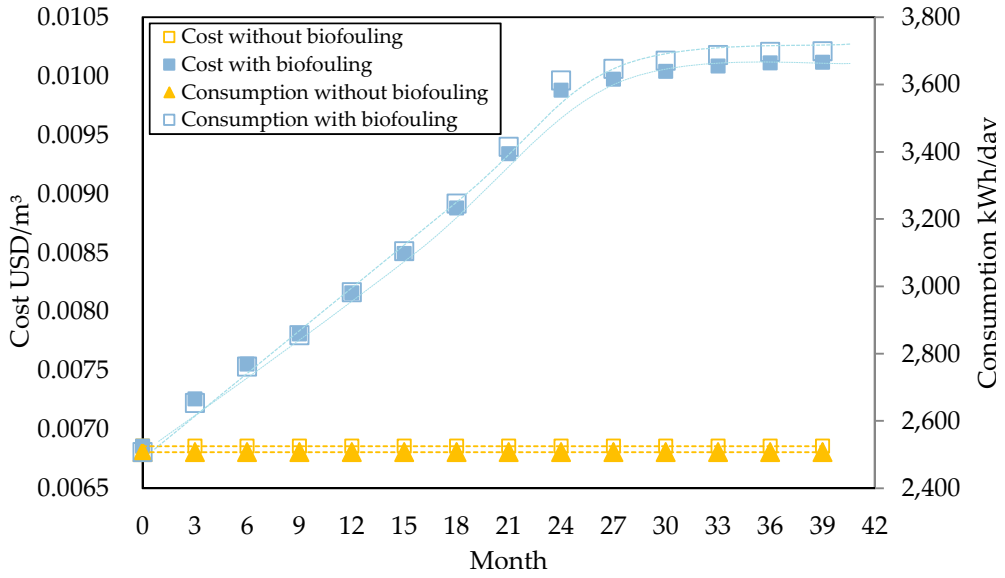


**Figure 9.** Daily consumption, in kilowatt hours per day (kWh/day), and cost of pumping, in dollars per cubic meter (USD/m$^3$), for the Elevated Pumping Station of Rio Branco, including both a pumping system with and without golden mussel bioinfestation.

After 24 months of bioinfestation, the daily consumption of the pumping system stabilizes at a value of 3612 kWh/day, as opposed to the consumption of an uninfested (without biofouling) pumping system, which stabilizes at 2506 kWh/day. Similarly, the cost of pumping per m$^3$ presents a steep increase in the first 24 months of operation, showing an increase of up to 0.0030 USD/m$^3$ after colonization by the GM, which is equivalent to a 44% increase in costs.

The results show, for the first time, the damage caused by the GM with regard to energy efficiency. To date, there are no data on other biofouler mussels, especially zebra mussels (an invasive mussel in North America), that can help in the discussion of our data. However, there is a noticeable decrease in the energy efficiency of pumping systems caused by the GM, with an increase in cost of almost 46%, after 30 months of infestation. The data obtained here can also support the Ivancost database, helping to obtain more assertive conclusions about the ecosystem costs related to the GM. In the first report on the cost of invasions in Brazil, they point out the scarce economic data reported for invasive species. Both Adelino et al. (2021) [19] and Burlokova et al. [18] point to the increase in costs caused by bioinfestation also affecting ecosystem services.

## 4. Conclusions

The methodology used was appropriate for the analysis of energy efficiency related to the presence of the golden mussel (GM) in a water pumping system. The complexity of the methodology, including the use of classical equations and the construction of new ones, allowed all of the objectives of this work to be achieved, even without the analysis of all the variables commonly used in the calculation of energy efficiency. Shell growth increases in the first year, and after that period, it suffers reductions in growth rate of 50% per year, stabilizing after the third year of life. This growth rate was corroborated by data from the literature and provided validation for the methodology of proportional relations between the measures performed in the target GMs. This was the starting point for the construction of new equations (three new equations), which allowed for the construction of roughness and thickness curves for biofouling, proving for the first time the relationship between the three elements (shell growth, roughness, and thickness of biofouling). The interference

of hydrodynamic drag (flow velocity) was fundamental for the above conclusion, since it causes the detachment of individuals, interfering with the progression of GM fixation (biofouling thickness). In fact, the thickness of the biofouling suffers velocity interference, and this has also been pointed out in the literature. In this study, we show that velocities above 3.8 m/s prevented increased biofouling thickness. This is important for the definition of mussel control and management strategies in pumping systems by controlling flow velocity. Another relevant point was that the size of the individuals did not directly interfere with the increase in roughness, but rather, with the formation of colonies (increased density, number of individuals/cm$^2$). This was especially the case for pipes of smaller diameter, where the increase in density represented a large increase in the load loss factor, proving that bioinfestation (an increase in biofouling thickness) causes a reduction in the efficiency of the pumping system by decreasing the flow diameter. This reduction in diameter causes an increase in energy consumption so that the same flow is achieved. We consider the cost of biofouling for other industrial plant systems, for example, to be much higher than that presented here (almost 46% for 30 months of infestation), since the calculations were made for only one water treatment plant, with simple mechanical fluid systems (when compared with an HPP, for example) and without taking into account localized losses, which would cause an even greater increase in the costs of pumping. As an alternative to the problem presented, performing stops during the operation of the pumping system for corrective maintenance would be the first option, avoiding an increase in operational costs. Another option could be adopting selective pumping criteria, which prioritize pumps and systems with larger diameters, since these are less impacted by GM biofouling. The application of this strategy in our case study could have meant a reduction in the operation time of Pump 3, since this pump is connected to a pipe with a smaller diameter (300 mm) than the other two pumps studied. To compensate, Pumps 1 or 2 could stay activated for a longer time. This way, the pump that was most affected by the bioinfestation, Pump 3, could serve as a backup. Measures such as regular pumping system inspections reduce the advancement of GM bioinfestation, preventing an increase in operational costs. Considering that this study focuses on the water supply and distribution sectors of the Amazon region, we call attention to the negative impacts of GM bioinfestation and provide possible ways to deal with this situation. Linked to these characteristics, bioinvasion would be very harmful for this type of pumping system, due to the morphology of the uptake and the difficulty of maintenance. Here, we provide results that demonstrate the energy efficiency of pumping systems impacted by the golden mussel.

**Supplementary Materials:** The following supporting information can be downloaded at: https://www.mdpi.com/article/10.3390/en16041858/s1.

**Author Contributions:** Conceptualization, T.R.C.d.S., R.O.P.S., T.H.D.A.V., A.S.B. and C.B.M.; Formal Analysis, T.R.C.d.S., T.H.D.A.V. and C.B.M.; Investigation, T.R.C.d.S., R.O.P.S. and C.B.M.; Metodology, T.R.C.d.S., J.T.M.d.A., R.O.P.S. and C.B.M.; Project Administration, T.R.C.d.S. and C.B.M.; Supervision, T.R.C.d.S., T.H.D.A.V., E.M.d.F.V. and C.B.M.; Validation, T.R.C.d.S. and C.B.M.; Visualization, T.R.C.d.S., A.S.B. and C.B.M.; Essay—Original Draft, T.R.C.d.S. and C.B.M.; Essay—proofreading and editing, T.R.C.d.S., J.T.M.d.A., E.M.d.F.V. and C.B.M. All authors have read and agreed to the published version of the manuscript.

**Funding:** This research was funded by CNPq—license number PQ: 304370/2018-5/305059/2022-0; Fapemig—license number PPM-00252-18; SEFAC/ANEEL—license number PD-06899-2912/2016 and this study was financed in part by the Coordenação de Aperfeiçoamento de Pessoal de Nível Superior—Brasil (CAPES)—Finance Code 001.

**Data Availability Statement:** The data presented in this study are available in article or supplementary material.

**Conflicts of Interest:** The authors declare no conflict of interest.

## Abbreviations

| | |
|---|---|
| ABNT | Brazilian Technical Standard |
| ASTM | American Society for Testing and Materials |
| CI | Cast iron |
| EPS | Elevated pumping station |
| GM | Golden mussel |
| HDPE | High-density polyethylene |
| HPP | Hydroelectric power plant |
| *L. fortunei* | *Limnoperna fortunei* |
| PVC | Polyvinyl chloride |
| Sin | Sine |
| Inf | Infestation |
| Op | Operation |
| Incr. | Increment |

## Nomenclature

| | |
|---|---|
| A | Area |
| bt | Biofouling thickness |
| C1 | Pumping system consumption |
| C2 | Pumping system consumption |
| C3 | Incremental consumption |
| C4 | Incremental costs |
| C5 | Daily costs |
| C6 | Total cost per trimester |
| C7 | Pumping cost |
| D | Diameter |
| $D_{vd}$ | Daily flow deficit |
| e | Roughness |
| f | Load loss factor |
| g | Gravity |
| H | Discharge head |
| $\Delta H$ | Load loss |
| $H_{total}$ | Total height of elevation |
| L | Length |
| mca (m $H_2O$) | Meters of water |
| P | Powe |
| $P_{pump}$ | Power of the pump |
| Q | Flow |
| $R_a$ | Average roughness |
| Re | Reynolds number |
| bs | Shell base |
| sh | Shell height |
| sl | Shell length |
| V | Velocity |
| $\gamma$ | Water-specific weight |
| $\varkappa$ | Kinematic viscosity of water |
| $\eta$ | Energy yield |
| $\Theta$ | Fixation angle |
| ind/$cm^2$ | Individuals per square centimeter |
| L/s | Liters per second |
| m/s | Meters per second |
| kW | Kilowatt |
| kWh | Kilowatt hour |
| $m^2$ | Square meters |
| $m^3$ | Cubic meters |
| mm | Millimeters |
| n | Number of constants |

| | |
|---|---|
| $B_1$ | First root of the Buzzelli equation |
| $B_2$ | Second root of the Buzzelli equation |
| log | Logarithm |
| ln | Neperian logarithm |
| $T_{ab}$ | Additional pumping time |

## References


1. Nakano, D.; Strayer, D.L. Biofouling animals in fresh water: Biology, impacts, and ecosystem engineering. *Front. Ecol. Environ.* **2014**, *12*, 167–175. [CrossRef] [PubMed]
2. Xu, M.; Darrigran, G.; Wang, Z.; Zhao, N.; Lin, C.C.; Pan, B. Experimental study on control of *Limnoperna fortunei* biofouling in water transfer tunnels. *J. Hydro-Environ. Res.* **2015**, *9*, 248–258. [CrossRef]
3. Cataldo, D.H. Larval Development of *Limnoperna Fortunei*. In *Limnoperna Fortunei*; Boltovskoy, D., Ed.; Invading Nature—Springer Series in Ecology of Invasions; Springer: Cham, Switzerland, 2015; Volume 10. [CrossRef]
4. Choi, S.S.; Chin, C.N. Study on the early development and larvae of Limnoperna fortunei. *Korean J. Malacol.* **1985**, *1*, 5–12.
5. Boltovskoy, D.; Morton, B.; Correa, N.; Cataldo, D.; Damborenea, C.; Penchaszadeh, P.E.; Sylvester, F. Reproductive Output and Seasonality of Limnoperna fortunei. In *Limnoperna Fortunei*; Boltovskoy, D., Ed.; Invading Nature—Springer Series in Ecology of Invasions; Springer: Cham, Switzerland, 2015; Volume 10, ISBN 978-3-319-13494-9. [CrossRef]
6. Darrigran, G.; Damborenea, M.C. Ecosystem Engineering Impact of Limnoperna fortunei in South America. *Zool. Sci.* **2011**, *28*, 1–7. [CrossRef] [PubMed]
7. Darrigran, G.; Agudo-Padrón, I.; Baez, P.; Belz, C.; Cardoso, F.; Carranza, A.; Collado, G.; Correoso, M.; Cuezzo, M.G.; Fabres, A.; et al. Non-native mollusks throughout South America: Emergent patterns in an understudied continent. *Biol. Invasions* **2020**, *22*, 853–871. [CrossRef]
8. Barbosa, N.P.; Ferreira, J.A.; Nascimento, C.A.; Silva, F.A.; Carvalho, V.A.; Xavier, E.R.; Ramon, L.; Almeida, A.C.; Carvalho, M.D.; Cardoso, A.V. Prediction of future risk of invasion by Limnoperna fortunei (Dunker, 1857) (Mollusca, Bivalvia, Mytilidae) in Brazil with cellular automata. *Ecol. Indic.* **2018**, *92*, 30–39. [CrossRef]
9. Campos, M.; Andrade, A.; Kunzmann, B. Modelling of the potential distribution of Limnoperna fortunei (Dunker, 1857) on a global scale. *Aquat. Invasions* **2014**, *9*, 253–265. [CrossRef]
10. National Energy Balance 2022. Available online: http://www.epe.gov.br (accessed on 10 August 2022).
11. Boltovskoy, D.; Correa, N.; Cataldo, D.; Sylvester, F. Dispersion and Ecological Impact of the Invasive Freshwater Bivalve Limnoperna fortunei in the Río de la Plata Watershed and Beyond. *Biol. Invasions* **2006**, *8*, 947–963. [CrossRef]
12. Oliveira, M.D.; Campos, M.C.S.; Paolucci, E.M.; Mansur, M.C.D.; Hamilton, S.K. Colonization and Spread of Limnoperna fortunei in South America. In *Limnoperna Fortunei*; Boltovskoy, D., Ed.; Invading Nature—Springer Series in Ecology of Invasions; Springer: Cham, Switzerland, 2015; Volume 10. [CrossRef]
13. Boltovskoy, D.; Xu, M.; Nakano, D. Impacts of Limnoperna Fortunei on Man-Made Structures and Control Strategies: General Overview. In *Limnoperna Fortunei*; Boltovskoy, D., Ed.; Invading Nature—Springer Series in Ecology of Invasions; Springer: Cham, Switzerland, 2015; Volume 10, ISBN 978-3-319-13494-9. [CrossRef]
14. GPS (Pipeline Study Group). *Biology of Golden Mussel (Limnoperna fortunei). Animal's Use and Prevention*; Institute of Aquatic Organisms of the Chinese Academy of Sciences: Wuhan, China, 1973; pp. 33–36.
15. Simeão, C.; De Resende, M.F.; Martinez, C.B. Variação das Características Hidráulicas em Condutos Forçados Operando sob Condições de Infestação por Limnoperna fortunei. *RBRH* **2011**, *16*, 13–24. [CrossRef]
16. Usher, K.M.; Kaksonen, A.H.; Cole, I.; Marney, D. Critical review: Microbially influenced corrosion of buried carbon steel pipes. *Int. Biodeterior. Biodegrad.* **2014**, *93*, 84–106. [CrossRef]
17. de Castro, A.L.P.; Serrano, R.O.P.; Pinto, M.A.; da Silva, G.H.T.; Ribeiro, L.D.A.; Viana, E.M.D.F.; Martinez, C.B. Case study: Abrasive capacity of Limnoperna fortunei (golden mussel) shells on the wear of 3 different steel types. *Wear* **2019**, *12*, 438–439. [CrossRef]
18. Burlakova, L.E.; Karatayev, A.Y.; Boltovskoy, D.; Correa, N.M. Ecosystem services provided by the exotic bivalves Dreissena polymorpha, D. rostriformis bugensis, and Limnoperna fortunei. *Hydrobiologia* **2022**, 1–44. [CrossRef] [PubMed]
19. Adelino, J.R.P.; Heringer, G.; Diagne, C.; Courchamp, F.; Faria, L.D.B.; Zenni, R.D. The economic costs of biological invasions in Brazil: A first assessment. *Neobiota* **2021**, *67*, 349–374. [CrossRef]
20. Diagne, C.; Leroy, B.; Gozlan, R.E.; Vaissière, A.-C.; Assailly, C.; Nuninger, L.; Roiz, D.; Jourdain, F.; Jarić, I.; Courchamp, F. InvaCost, a public database of the economic costs of biological invasions worldwide. *Sci. Data* **2020**, *7*, 277. [CrossRef] [PubMed]
21. Koutsandreas, D.; Kleanthis, N.; Flamos, A.; Karakosta, C.; Doukas, H. Risks and mitigation strategies in energy efficiency financing: A systematic literature review. *Energy Rep.* **2022**, *8*, 1789–1802. [CrossRef]
22. Patterson, M.G. What is energy efficiency? *Energy Policy* **1996**, *24*, 377–390. [CrossRef]
23. Oikonomou, K.; Parvania, M.; Khatami, R. Optimal Demand Response Scheduling for Water Distribution Systems. *IEEE Trans. Ind. Inform.* **2018**, *14*, 5112–5122. [CrossRef]
24. Dadar, S.; Đurin, B.; Alamatian, E.; Plantak, L. Impact of the Pumping Regime on Electricity Cost Savings in Urban Water Supply System. *Water* **2021**, *13*, 1141. [CrossRef]

25. Martin-Candilejo, A.; Santillán, D.; Iglesias, A.; Garrote, L. Optimization of the Design of Water Distribution Systems for Variable Pumping Flow Rates. *Water* **2020**, *12*, 359. [CrossRef]
26. Hajibabaei, M.; Nazif, S.; Sereshgi, F.T. Life cycle assessment of pipes and piping process in drinking water distribution networks to reduce environmental impact. *Sustain. Cities Soc.* **2018**, *43*, 538–549. [CrossRef]
27. Hu, J.; Dong, H.; Xu, Q.; Ling, W.; Qu, J.; Qiang, Z. Impacts of water quality on the corrosion of cast iron pipes for water distribution and proposed source water switch strategy. *Water Res.* **2017**, *129*, 428–435. [CrossRef] [PubMed]
28. Shankar, A.R.; Anandkumar, B.; Thinaharan, C.; George, R.P.; Rooby, J.; Philip, J.; Mudali, U.K. Corrosion Evaluation of Buried Cast Iron Pipes Exposed to Fire Water System for 30 years. *Trans. Indian Inst. Met.* **2019**, *73*, 9–21. [CrossRef]
29. Mahato, A.C.; Ghoshal, S.K. Energy-saving strategies on power hydraulic system: An overview. *Proc. Inst. Mech. Eng. Part I J. Syst. Control. Eng.* **2021**, *235*, 147–169. [CrossRef]
30. Morales-Hernández, M.; Playán, E.; Latorre, B.; Montoya, F.; Madurga, C.; de Rivera, A.S.; Zapata, N. Normalized pressure: A key variable to assess zebra mussel infestation in pressurized irrigation networks. *Agric. Water Manag.* **2022**, *260*, 107300. [CrossRef]
31. Moody, L.F. Friction factors for pipe flow. *Trans. AMSE* **1944**, *66*, 671–684. [CrossRef]
32. Colebrook, C.F.; White, C.M. The Reduction of Carrying Capacity of Pipes with Age. *J. Inst. Civ. Eng.* **1937**, *7*, 99–118. [CrossRef]
33. Mohebbi, H.; Li, C.Q. Experimental Investigation on Corrosion of Cast Iron Pipes. *Int. J. Corros.* **2011**, *2011*, 506501. [CrossRef]
34. Lucio, F.D.S.; Xavier, G.B.; Mesquita, A.A.; Moreira, J.G.D.V.; Dos Santos, W.L.; Serrano, R.O.P. Granulometric and morphological variation of the bottom sediments of the Acre River: Initial contributions to the hydrosedimentological study of a river channel in the southeastern Amazon. *UÁQUIR* **2020**, *2*, 80–98. [CrossRef]
35. Serrano, R.O.P.; Santos, L.P.; Viana, E.M.D.F.; Pinto, M.A.; Martinez, C.B. Case study: Effects of sediment concentration on the wear of fluvial water pump impellers on Brazil's Acre River. *Wear* **2018**, *408–409*, 131–137. [CrossRef]
36. DEPASA. ECA Report. Available online: https://www.ac.gov.br (accessed on 3 March 2022).
37. Garton, D.W.; Johnson, L.E. Variation in growth rates of the zebra mussel, *Dreissena polymorpha*, within Lake Wawasee. *Freshw. Biol.* **2000**, *45*, 443–451. [CrossRef]
38. Nakano, D.; Kobayashi, T.; Sakaguchi, I. Population dynamics and growth of *Limnoperna fortunei*. In *Limnoperna Fortunei*; Boltovskoy, D., Ed.; Invading Nature—Springer Series in Ecology of Invasions; Springer: Cham, Switzerland, 2015; Volume 10, ISBN 978-3-319-13494-9. [CrossRef]
39. Boltovskoy, D.; Cataldo, D.H. Population dynamics of *Limnoperna fortunei*, an invasive fouling mollusc, in the lower Parana river (Argentina). *Biofouling* **1999**, *14*, 255–263. [CrossRef]
40. Darrigran, G.; Maroñas, M. Crecimiento valvar de *Limnoperna fortunei* (Dunker, 1857) (Mytilidae) de una localidad de clima templado de la regionión neotropical. In: Darrigran, G.; Bonel, N.; Colautti, D.; Cazzaniga, N.J. An Alternative Method to Assess Individual Growth of the Golden Mussel (*Limnoperna fortunei*). *Wild J. Freshw. Ecol.* **2002**, *26*, 527–535. [CrossRef]
41. Mackie, G.L.; Claudi, R. *Monitoring and Control of Macrofouling Mollusks in Freshwater Systems*; CRC Press: New York, NY, USA, 2010; ISBN 978-04-2914-964-1. (In Portuguese)
42. Fróes, C.L.; Duarte, M.S.C.; Branco, J.R.T. Estudo morfológico das estruturas envolvidas no mecanismo de adesão do Limnoperna fortunei (Dunker, 1857). *Rev. Agrogeoambiental* **2012**, *4*, 1–10. [CrossRef]
43. *ABNT NBR 10007*; Association of Technical Standards: Sampling of Solid Waste. 2004, pp. 1–21. Available online: https://wp.ufpel.edu.br (accessed on 23 April 2022).
44. Simeon, C.M.G. Influence of the variation of speed and pressure on *Limnoperna fortunei* Dunker, 1857 (Bivalvia, Mytilidae) and verification of the effects of latex toxicity of Euphorbia splendens Var hislopii N.E.B. (Euprorbiaceae) for this species. Ph.D. Thesis, Federal University of Minas Gerais, Belo Horizonte, Brazil, 2011.
45. Castro, A.L.P. Study of speeds and Reynolds number for the detachment of the golden mussel (*Limnoperna fortunei*). Ph.D. Thesis, Federal University of Minas Gerais, Belo Horizonte, Brazil, 2013.
46. Adams, T.; Grant, C.; Watson, H. A Simple Algorithm to Relate Measured Surface Roughness to Equivalent Sand-grain Roughness. *Int. J. Mech. Eng. Mechatronics* **2012**, *1*, 66–71. [CrossRef]
47. Robertson, R.H.S.; Emödi, B.S. Rugosity of Granular Solids. *Nature* **1943**, *152*, 539–540. [CrossRef]
48. Han, X.; Kang, Y.; Li, D.; Zhao, W. Effects of surface roughness on self-excited cavitating water jet intensity in the organ-pipe nozzle: Numerical simulations and experimental results. *Mod. Phys. Lett. B* **2019**, *33*, 39. [CrossRef]
49. Mataix, C. *Hydraulic Turbochargers*; Universidad Pontificia Comillas: Madrid, Spain, 2009; ISBN 978-84-8468-252-3.
50. Buzzelli, D. Calculating friction in one step. *Mach. Des.* **2008**, *80*, 54–55.
51. Kaya, D.; Kılıç, F.; Öztürk, H.H. Energy Efficiency in Pumps. In *Energy Management and Energy Efficiency in Industry*; Springer: Cham, Switzerland, 2021; pp. 329–374. [CrossRef]
52. Xu, M.; Cao, X.W.; Wang, Z.Y.; Wang, X.Z. Attachment characteristics of golden mussels (*Limnoperna fortunei*) in water transport projects. *J. Tsinghua Univ. [Qinghua Daxue Xuebao]* **2012**, *52*, 170–176. (In Chinese)
53. ANEEL: Residual Tariffs. Available online: https://app.powerbi.com (accessed on 9 June 2022).
54. BCB: Quotes and Newsletters. Available online: https://www.bcb.gov.br (accessed on 9 June 2022).